A Detailed Analytical Analysis on the Dynamic Behaviour of a MEMS Vibrating Internal Ring Gyroscope

Waqas Amin Gill *, Ian Howard, Ilyas Mazhar, Kristoffer McKee *

Posted Date: 17 July 2024

doi: 10.20944/preprints202407.1366.v1

Keywords: MEMS; MEMS Gyroscope; Vibrating Ring Gyroscope; Dynamics; Motion Equations; Resonance Frequency; Ring Resonator; Inertial Sensor

Article

A Detailed Analytical Analysis on the Dynamic Behaviour of a MEMS Vibrating Internal Ring Gyroscope

Waqas Amin Gill *, Ian Howard, Ilyas Mazhar and Kristoffer McKee *

Department of Mechanical Engineering, Curtin University, Perth, WA 6845, Australia; i.howard@exchange.curtin.edu.au (I.H.); i.mazhar@curtin.edu.au (I.M.)

* Correspondence: waqasgill80@live.com (W.A.G.); k.mckee@curtin.edu.au (K.M.)

Abstract: This paper presents the development of an analytical model of Microelectromechanical Systems (MEMS) internal vibrating ring gyroscope. The internal ring structure consists of eight semicircular beams that are attached to the externally placed anchors. The research work analyses the vibrating ring gyroscope inplane displacement behavior and the resulting elliptical vibrational modes. The elliptical vibrational modes appear as pairs with the same resonance frequency due to the symmetric structure of the design. The analysis commences by conceptualizing the ring as a geometric structure with a circular shape, possessing specific dimensions such as thickness, height, and radius. We construct a linear model that characterizes the vibrational dynamics of the internal vibrating ring. The analysis develops a comprehensive mathematical formulation for the radial and tangential displacements in local polar coordinates, considering the inextensional displacement of the ring structure. By utilizing the derived motion equations, we highlight the underlying relationships driving the vibrational characteristics of the MEMS vibrating ring gyroscope. These dynamic vibrational relationships are essential in enabling the vibrating ring gyroscope's future utilization in accurate navigation and motion sensing technologies.

Keywords: MEMS; MEMS gyroscope; vibrating ring gyroscope; dynamics; motion equations; resonance frequency; ring resonator; inertial sensor

1. Introduction

Microelectromechanical systems (MEMS) inertial sensors have become integral to many modern-day smart devices because of their micro size, energy efficiency, low cost, and high-performance characteristics [1–7]. Among the various MEMS inertial sensors, vibrating ring gyroscopes stand out as imminent inertial sensors that are extensively used in many applications to measure and control the position of the system. Their usage has increased tremendously in smart electronics, automotive, military, biomedical, and space applications[8–17].

As the world's demand is seeking towards the down scaling and improving performances of these microscale inertial sensors. To the development of the high-performance devices, it is important to understand the dynamic behaviour of these sensors in different environments. Most MEMS vibrating gyroscopes operate on the translational motion principle of a single-proof mass system. Because of the single-proof mass system, translational motion delivers excellent gyroscopic performance with simple microfabrication processes. While some of the gyroscopes operate on the rotational motion of the spring-mass system, these systems require complex operational mechanisms and microfabrication processes.

MEMS vibrating ring gyroscopes, like other vibrating gyroscopes, operate on the fundamentals of the Coriolis effect [14,18–21]. The vibrating ring structure is set to continuously oscillate in the X and Y axes. These oscillations can be seen as elliptical shapes in the X and Y axes. The primary oscillation has four nodes where the vibrating ring has no displacement; these four nodes are located at 45 degrees between both axes. The vibrating ring primary oscillation dynamic system is shown in

 doi:10.20944/preprints202407.1366.v1

Figure 1. When the vibrating ring structure is exposed to the external rotation along the Z-axis (in this case), the secondary oscillation starts appearing in the sensing direction at 45 degrees between the X and Y axes due to the Coriolis force.

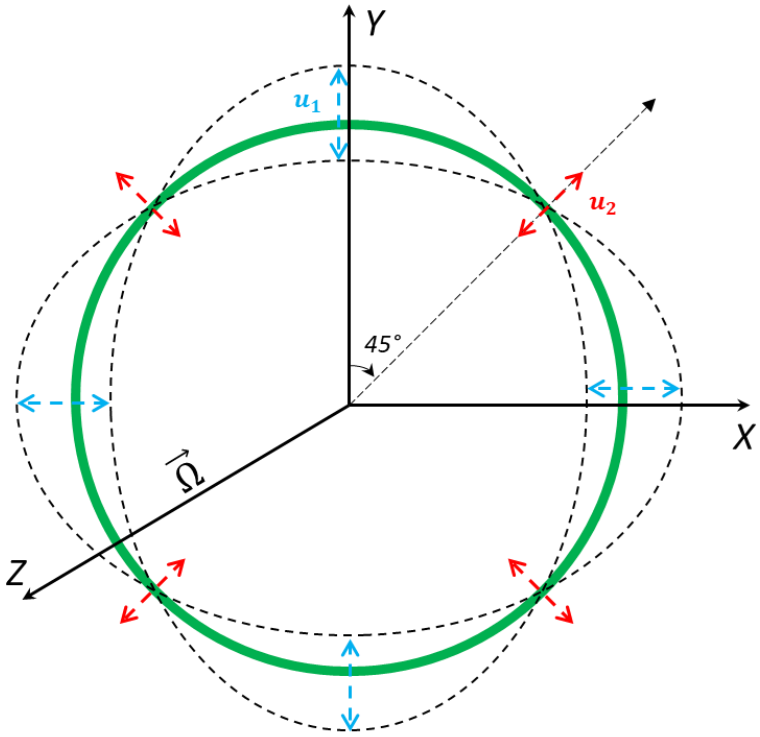

Figure 1. The dynamic illustration of the primary oscillation of the Vibrating ring gyroscope [22].

2. Dynamics of MEMS Vibrating Ring Gyroscope

The fundamental understanding of the dynamics of MEMS vibrating ring gyroscopes starts with a single vibrating ring mass system placed above the substrate. The ring structure is attached with flexible suspension beams and centrally placed anchor support. A linear vibrating ring gyroscope is required to oscillate in two adjacent axes with identical vibrational modes for the gyroscope's operation. Suppose the vibrating ring gyroscope drives along the X and Y axes with the displacement u_1 and when the gyroscope experiences rotation along the Z-axis, the displacement u_2 appears at 45 degrees between the X and Y axes, as shown in Figure 1. The dynamic system of a vibrating ring gyroscope is referred to as having two degrees of freedom.

The first and foremost task in analyzing the MEMS vibrating ring gyroscope's dynamic behavior is to study the effects of various forces on the gyroscope. In particular, the influence of the rotational-induced Coriolis force on the body in the inertial system and observations from a rotating reference frame. For determining the equations of forces acting on the system, it is necessary to examine the motion of an object in a rotating reference frame relative to an inertial reference frame. The inertial and non-inertial reference frames are explained in detail below and shown in Figure 2.

Preprints.org (www.preprints.org) | NOT PEER-REVIEWED | Posted: 17 July 2024 doi:10.20944/preprints202407.1366.v1

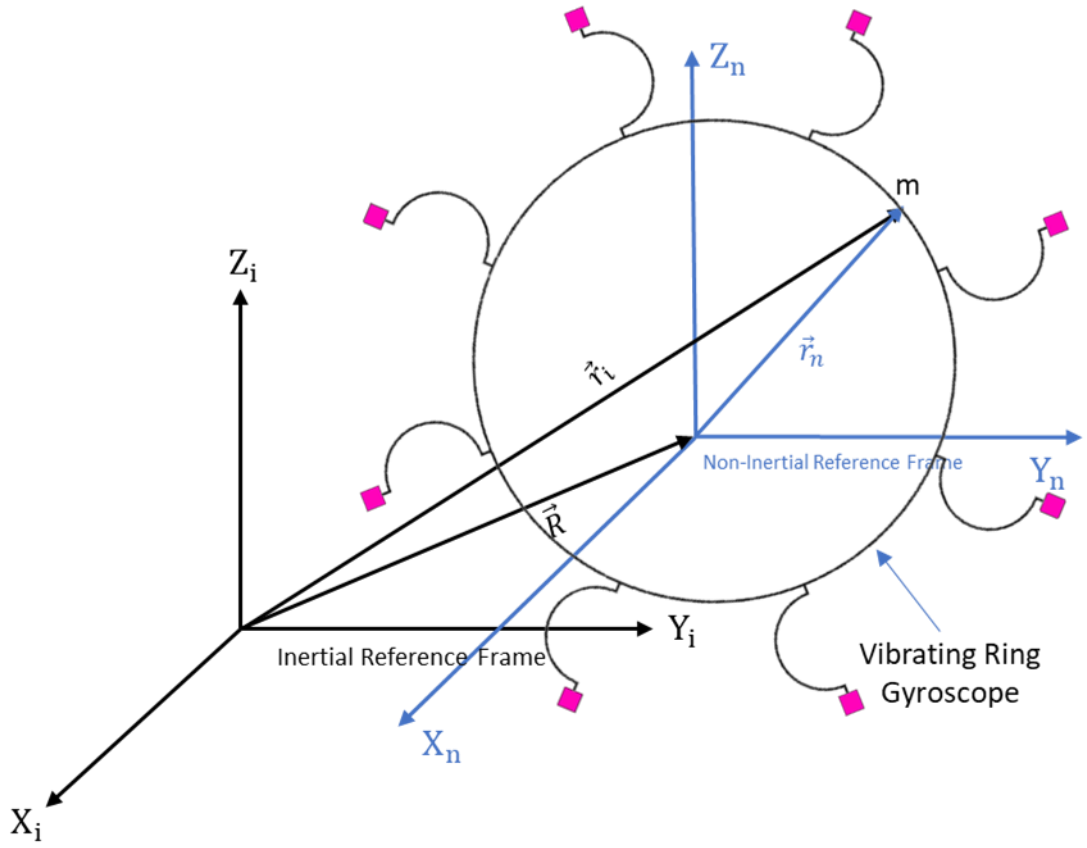

Figure 2. A schematic representation of Inertial and non-inertial reference frames with position vectors.

2.1. Reference Frames

Assuming a non-inertial rotating reference frame with constant acceleration relating to the inertial reference frame, we can start with Newton's second law of motion and determine the inertial force. The inertial reference frame and non-inertial reference frame with point mass "m" and position vectors are shown in Figure 2. The description of the elements is written below:

I_i = Inertial reference frame (stationary)

I_n = non-inertial reference frame (accelerating)

$\vec{R}$= position vector of non-inertial reference frame."I_n" with respect to the inertial frame "I_i"

$\dot{\vec{R}}$= velocity of non-inertial reference frame "I_n" with respect to "I_i"

$\ddot{\vec{R}}$= acceleration of non-inertial frame "I_n" with respect to "I_i"

$\vec{r_i}$= Position vector relative to the inertial reference frame

$\vec{r_n}$= Position vector relative to non-inertial reference frame

$\ddot{\vec{r_i}}$= acceleration of inertial reference frame

$\ddot{\vec{r_n}}$= acceleration of non-inertial reference frame

An observer from an inertial reference frame (stationary) can see a point mass "m" with a position vector $\vec{r_i}$ and hence the force acting on the inertial reference frame is given as equation 1.

$$\vec{F} = m\ddot{\vec{r_i}} \quad (1)$$

We start with the position vectors and then take the second derivative of the position vectors.

Preprints.org (www.preprints.org) | NOT PEER-REVIEWED | Posted: 17 July 2024 doi:10.20944/preprints202407.1366.v1

$$r_i = R + r_n \quad (2)$$

$$r_i = R + r_n \quad (3)$$

Substitute equation 3 into equation 1.

$$F = m(R + r_n) \quad (4)$$

$$F - mR = mr_n \quad (5)$$

$$F - F_o = F_n \quad (6)$$

The force $\vec{F_o}$ is the inertial force observed from the non-inertial reference frame, $\vec{F}$ is the force which is observed from the inertial reference frame and $\vec{F_n}$ is the force from the non-inertial reference frame.

Let's consider a vector P that interacts with the time derivative of the inertial reference frame to the time derivative of the non-inertial reference frame. The vector P will rotate with angular velocity in a non-inertial reference frame with respect to the inertial reference frame and it is represented as equation 7.

$$\left(\frac{d}{dt}\vec{P}\right)_i = \left(\frac{d}{dt}\vec{P}\right)_n + \vec{\Omega} \times \vec{P} \quad (7)$$

Further, we will investigate the equation relating to the velocities in the inertial and non-inertial reference frames. By using equation 7 and considering the position vector $\vec{P} = \vec{r}$. The next step is to investigate equation 7 which relates to accelerations present in inertial and non-inertial reference frames.

$$\left(\frac{d}{dt}\right)_i \left(\frac{d\vec{r}}{dt}\right)_i = \left(\frac{d}{dt}\right)_n \left(\frac{d\vec{r}}{dt}\right)_i + \vec{\Omega} \times \left(\frac{d\vec{r}}{dt}\right)_i \quad (8)$$

As given in equation 7, the velocity observed by the inertial reference frame is equal to the velocity and angular velocity experienced by the non-inertial reference frame, it is $\left(\frac{d}{dt}\vec{r}\right)_i = \left(\frac{d}{dt}\vec{r}\right)_n + \vec{\Omega} \times \vec{r}$ and substitute into the equation 8.

$$\left(\frac{d^2\vec{r}}{dt^2}\right)_i = \left(\frac{d}{dt}\right)_n \left[\left(\frac{d\vec{r}}{dt}\right)_n + \vec{\Omega} \times \vec{r}_n\right] + \vec{\Omega} \times \left[\left(\frac{d\vec{r}}{dt}\right)_n + \vec{\Omega} \times \vec{r}_n\right] \quad (9)$$

$$\left(\frac{d^2\vec{r}}{dt^2}\right)_i = \left(\frac{d^2\vec{r}}{dt^2}\right)_n + \left(\frac{d}{dt}\right)_n (\vec{\Omega} \times \vec{r}_n) + \vec{\Omega} \times \left(\frac{d\vec{r}}{dt}\right)_n + \vec{\Omega} \times (\vec{\Omega} \times \vec{r}_n) \quad (10)$$

$$\left(\frac{d^2\vec{r}}{dt^2}\right)_i = \left(\frac{d^2\vec{r}}{dt^2}\right)_n + 2\vec{\Omega} \times \left(\frac{d\vec{r}}{dt}\right)_n + \vec{\Omega} \times (\vec{\Omega} \times \vec{r}_n) \quad (11)$$

Acceleration can be observed in the inertial reference frame is equal to acceleration in the non-inertial reference frame with Coriolis acceleration and centripetal acceleration.

Now consider the non-inertial reference frame with the inertial reference frame. A rotation "θ" is applied into the non-inertial reference frame and represented in Figure 3.

Preprints.org (www.preprints.org) | NOT PEER-REVIEWED | Posted: 17 July 2024 doi:10.20944/preprints202407.1366.v1

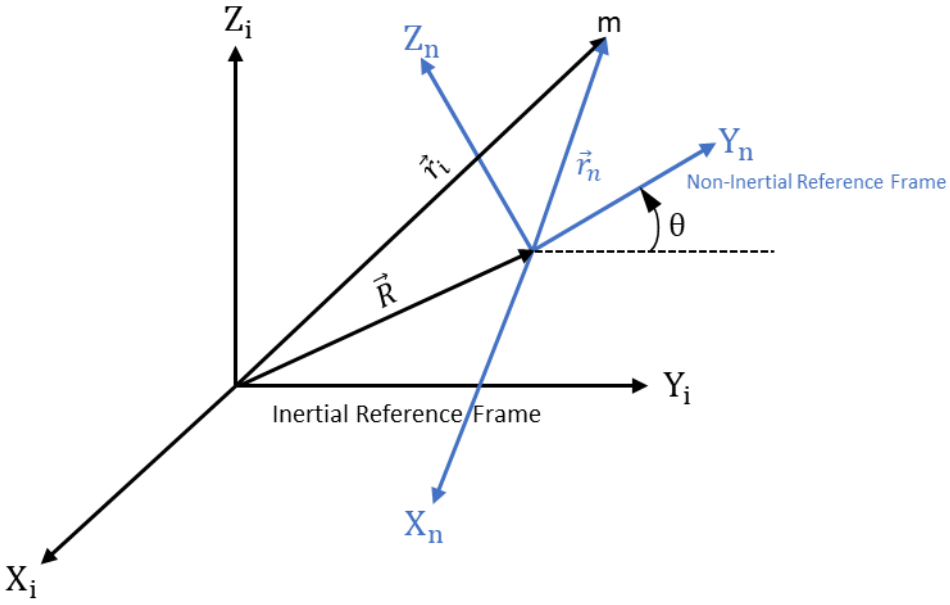

Figure 3. A schematic view of the position vector of a non-inertial reference frame with respect to an inertial reference frame with rotation applied.

$$\vec{r}_i = \vec{R} + \vec{r}_n \tag{2}$$

$$\left(\frac{d\vec{r}}{dt}\right)_i = \left(\frac{d\vec{R}}{dt}\right) + \left(\frac{d\vec{r}}{dt}\right)_n + \left(\frac{d\vec{\theta}}{dt} \times \vec{r_n}\right) \tag{12}$$

$$\begin{aligned}\left(\frac{d^2\vec{r}}{dt^2}\right)_i = &\left(\frac{d^2\vec{R}}{dt^2}\right) + \left(\frac{d^2\vec{r}}{dt^2}\right)_n + \left(\frac{d\theta}{dt}\right)_n \times \left(\frac{d\vec{r}}{dt}\right)_n \\ &+ \left(\frac{d\theta}{dt}\right)_n \times \left(\frac{d\vec{\theta}}{dt} \times \vec{r_n}\right) + \left(\frac{d^2\theta}{dt^2}\right) \times \vec{r_n} \\ &+ \left(\frac{d\theta}{dt}\right)_n \times \left(\frac{d\vec{r}}{dt}\right)_n\end{aligned} \tag{13}$$

$$\begin{aligned}\left(\frac{d^2\vec{r}}{dt^2}\right)_i = &\left(\frac{d^2\vec{R}}{dt^2}\right) + \left(\frac{d^2\vec{r}}{dt^2}\right)_n + \left(\frac{d\vec{\Omega}}{dt}\right) \times \vec{r_n} \\ &+ 2\vec{\Omega} \times \left(\frac{d\vec{r}}{dt}\right)_n + \vec{\Omega} \times \left(\vec{\Omega} \times \vec{r}_n\right)\end{aligned} \tag{14}$$

$$\ddot{\vec{r}}_i = \ddot{\vec{R}} + \ddot{\vec{r}}_n + \dot{\vec{\Omega}} \times \vec{r_n} + 2\vec{\Omega} \times \dot{\vec{r}}_n + \vec{\Omega} \times \left(\vec{\Omega} \times \vec{r}_n\right) \tag{15}$$

It is understood the concept of the dynamics of the gyroscope when we apply Newton's second law of motion equation on the acceleration with the gyroscope's mass as written in equations 16 and 17.

$$F = m\,\ddot{\vec{r}}_i \tag{16}$$

 doi:10.20944/preprints202407.1366.v1

$$F_A = m\left[\ddot{\vec{R}} + \ddot{\vec{r}}_n + \dot{\vec{\Omega}} \times \vec{r_n} + 2\vec{\Omega} \times \dot{\vec{r}}_n + \vec{\Omega} \times \left(\vec{\Omega} \times \vec{r}_n\right)\right] \quad (17)$$

Here F_A is the applied force on the reference frame, $\ddot{\vec{r}}_i$ is the acceleration experienced by the inertial reference frame, the combination of $(\ddot{\vec{R}} + \ddot{\vec{r}}_n + \dot{\vec{\Omega}} \times \vec{r_n})$ is the acceleration observed by the non-inertial reference frame, $\ddot{\vec{R}}$ is a linear acceleration observed in the non-inertial reference frame, $\ddot{\vec{r}}_n$ is the acceleration in the non-inertial reference frame, and $\vec{\Omega}$ does the non-inertial reference frame experience the angular velocity. The expression $\vec{\Omega} \times \left(\vec{\Omega} \times \vec{r}_n\right)$ is the centripetal acceleration and the expression $2\vec{\Omega} \times \dot{\vec{r}}_n$ is the Coriolis acceleration. The Coriolis acceleration is the main concept that transfers the rotational energy of the non-inertial reference frame for measuring the rotation rate with respect to the inertial reference frame.

2.2. Motion Equations of Vibrating Ring Gyroscope

The MEMS vibrating ring gyroscope is an inertial sensor that measures and control precise and accurate angular rate measurements in dynamic motion environments. Utilizing Coriolis force and resonant frequency principles, this miniaturized device offers excellent sensitivity and stability, ideal for applications such as navigation, stabilization, and motion tracking. Dual-axis gyroscopes, which measure angular motion in two orthogonal axes, tend to be larger and consume more power than the MEMS vibrating ring gyroscope. The MEMS vibrating ring gyroscope perform better than dual-axis and tuning fork gyroscopes in several key aspects, including size, power consumption, sensitivity, and reliability. Its symmetrical design and operating principles make it a highly attractive sensor for various applications, including navigation, stabilization, and motion tracking[23–25].

In this section, we present the development of a linear mechanical model for a vibrating ring resonator. The ring structure consists of eight semicircular support springs that are connected with the fixed anchor support [26–30]. The vibrational mode shapes characterise the oscillations of the ring. In the case of symmetric design structures, such as vibrating ring, it is observed that mode shapes appear in pairs comprising identical resonance frequencies and being oriented orthogonally to each other.

2.2.1. Coordinates for Vibrating Ring Gyroscope

A proposed MEMS vibrating internal ring resonator with eight semicircular beams connected to the externally placed anchors makes a complete vibrating ring gyroscope, as shown in Figure 4. In this study, we will consider inplane displacements of the vibrating ring and evaluate the elliptical vibrational modes. A vibrating ring gyroscope possesses a symmetric design structure, so the vibrational modes occur in identical pairs with the same resonance frequency.

 doi:10.20944/preprints202407.1366.v1

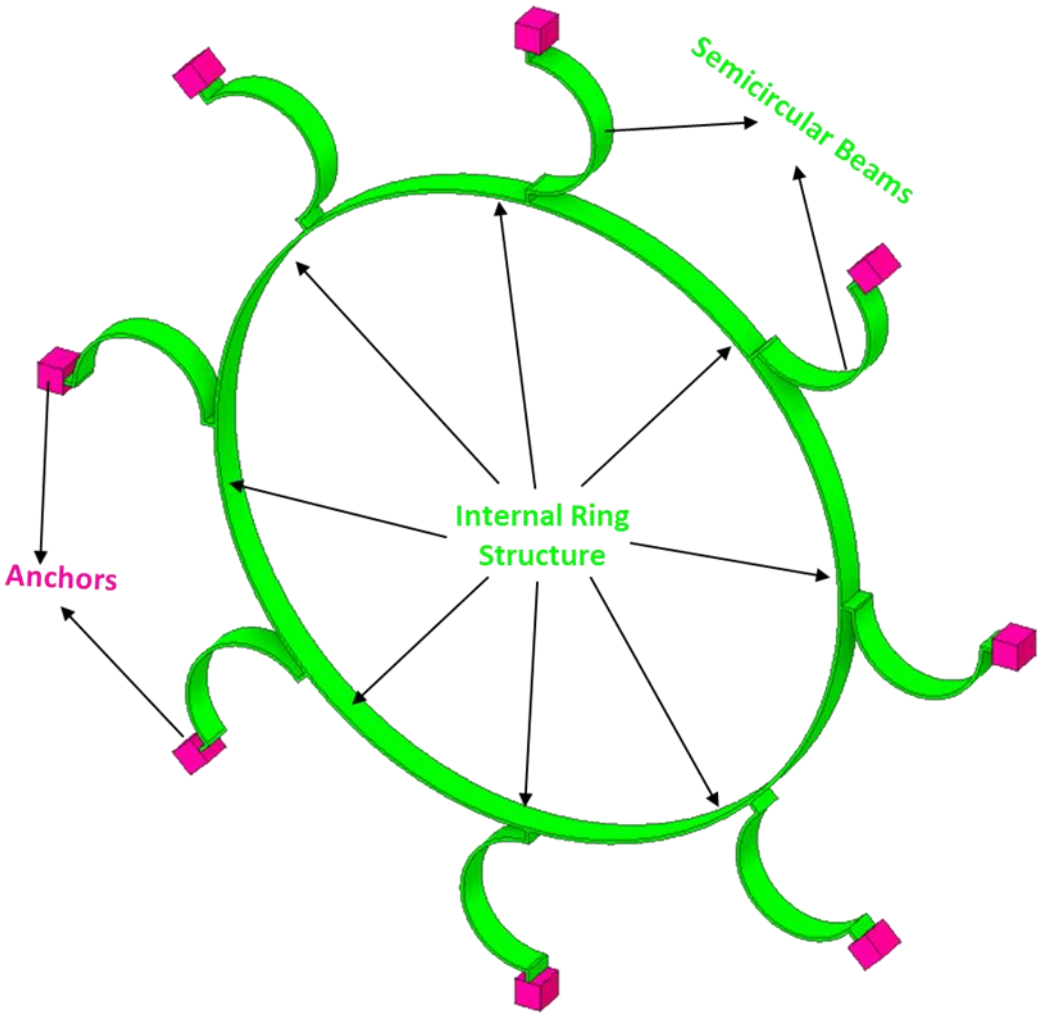

Figure 4. A schematic view of the internal vibrating ring gyroscope.

Firstly, the vibrating ring is considered as a perfect round ring with thickness "t". The cross-sectional area of the ring is shown in Figure 5. Where "h" is height, R is the radius of the ring center line, "t" is the thickness of the ring, and "A" is the cross-sectional area of the ring. The ring's displacement and elastic deformation are relatively small, so it is considered as a linear model of the vibrating ring gyroscope.

 doi:10.20944/preprints202407.1366.v1

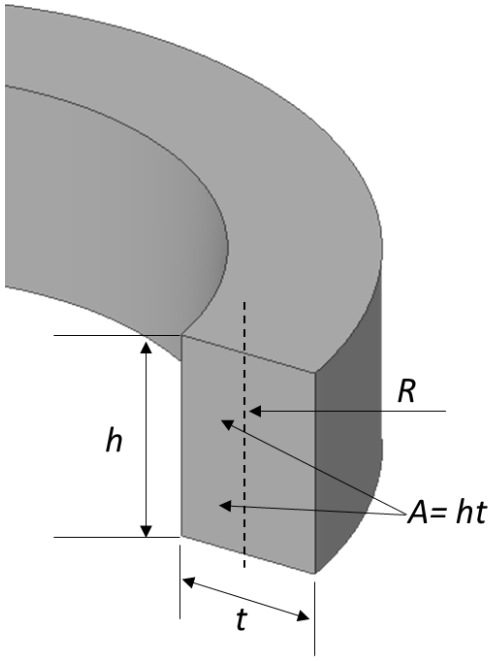

Figure 5. A cross-sectional area "A" of the ring structure with the centreline radius "R", height "h", and thickness "t".

The analysis starts with ring motion and consider the elliptical vibrational mode only, which is also represented by 2θ. The inplane vibrations of a vibrating ring are shown in Figure 6. Each infinitesimal element inplane vibration possesses two degrees of freedom. The displacements can be characterized in local polar coordinates using the variables. u_1 and u_2. Under the assumption of inextensional displacement of the ring. The radial displacement u_1 and tangential displacement u_2 of the ring in relation to the mid-section of the ring at a specific ring angle α can be expressed as equations 18 and 19.

$$u_1(\alpha) = G_1 \cos\ (2\alpha) + G_2 \sin\ (2\alpha) \tag{18}$$

$$u_2(\alpha) = \frac{G_1}{2} \sin\ (2\alpha) - \frac{G_2}{2} \sin\ (2\alpha) \tag{19}$$

Preprints.org (www.preprints.org) | NOT PEER-REVIEWED | Posted: 17 July 2024 doi:10.20944/preprints202407.1366.v1

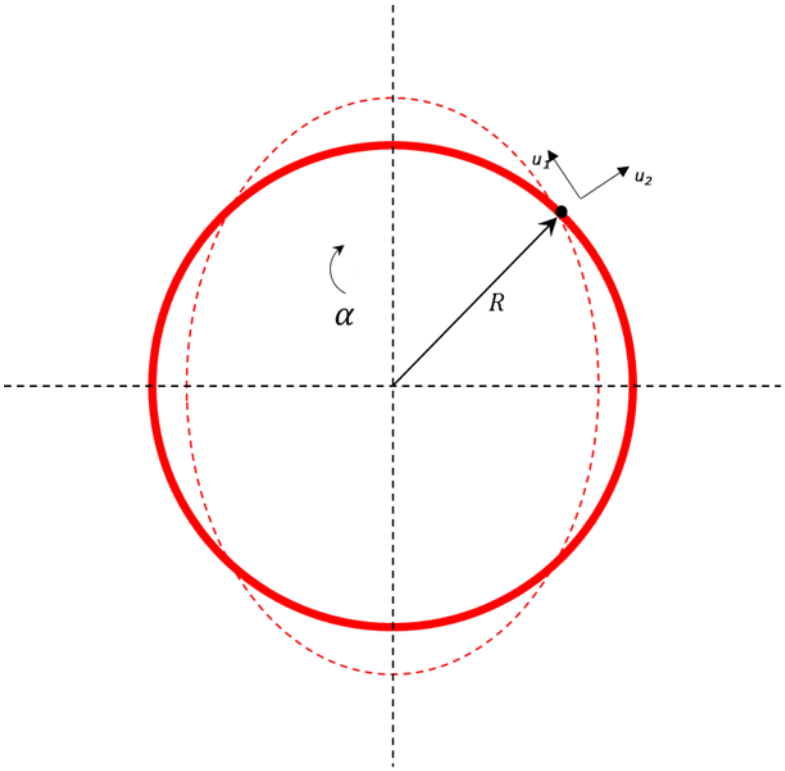

Figure 6. The displacement of the inplane ring as an elliptical mode of vibration.

2.2.2. Various Energies Effect

To understand the motion equations of the vibrating ring structure, we will evaluate the effects of various energies on the ring resonator and the elliptical mode of vibration of the ring structure. Also, considered as the coordinates of 2θ elliptical vibrations, as shown in Figure 6. The Lagrange equation is considered to determine the motion equation for the vibrating ring gyroscope. The given scheme of the energy equation is shown below. Here L represents the Lagrange equation, which is $L = K_E - (R_E + U_E + U_{SC})$. Where K_E is the kinetic energy, R_E is the Rayleigh damping, U_E is the strain energy and U_{SC} is the strain energy of the semicircular support beams.

$$\frac{d}{dt}\left(\frac{\partial K_E}{\partial \dot{e}_i}\right) - \frac{\partial K_E}{\partial e_i} - \frac{\partial R_E}{\partial \dot{e}_i} - \frac{\partial (U_E + U_{SC})}{\partial e_i} = \frac{\partial E_i}{\partial e_i}, (i = 1,2, \dots, n) \tag{20}$$

Kinetic Energy

To find the kinetic energy of the vibrating ring, it is to consider the displacements of the ring and the central anchor. The absolute displacements of the ring are denoted by u_1 and u_2 and for the central anchor, denoted as x_a and y_a. To determine the absolute displacements denoted as x and y of the vibrating ring system, it needs to combine the displacements terms of the vibrating ring and centrally placed anchor. The absolute velocities $v_1$and v_2 of the ring are given in equations 21 and 22.

$$v_1 = \frac{dx}{dt} = \frac{du_1}{dt} cos\alpha + \frac{du_2}{dt} sin\alpha + \frac{dx_a}{dt} \tag{21}$$

$$v_2 = \frac{dy}{dt} = \frac{du_2}{dt} cos\alpha - \frac{du_1}{dt} sin\alpha + \frac{dy_a}{dt} \tag{22}$$

Hence, the kinetic energy of the vibrating ring is written as equation (23)

$$K_E = \frac{1}{2} A\rho R \int_0^{2\pi} ({v_1}^2 + {v_2}^2)\, d\alpha \tag{23}$$

 doi:10.20944/preprints202407.1366.v1

Here ρ is the density, R is the radius, and A is the cross-sectional area of the vibrating ring gyroscope. By substituting equations 21 and 22 in equation 23 and then further solving it. It is found out the kinetic energy of the ring as equation 24 where m represents the mass of the vibrating ring.

$$K_E = \frac{1}{2}m\left[\frac{5}{8}\left(\frac{dG_1}{dt}\right)^2 + \frac{5}{8}\left(\frac{dG_2}{dt}\right)^2\right] \tag{24}$$

Equation 24 provides a detailed dynamic movement of the ring through the kinetic energy equation. The equation considered both the rigid body displacement of the ring and the elliptical mode of the ring structure, which pertain to the displacements with inplane of the motion of the ring. Moreover, the equation considers the influence of base excitation that refers to external forces applied on the anchors. The important feature is the decoupling of the generalized coordinates G_1 and G_2 that represent the motion of the ring. The coordinates in the equation are not mutually dependent in calculating kinetic energy. The phenomenon of uncoupling suggests that the various components of motion, such as inplane vibrations and base excitation contribute to the overall kinetic energy of the vibrating ring gyroscope system.

Elastic Strain Energy

In relation to the concept of the elastic strain energy, it is supposed that the vibrating ring possesses elastic properties and corresponds to Hook's law. The law states that stress is directly proportional to strain with constant proportionality being Young's Modulus "E" for the material. Hence the elastic strain energy "U_E" is.

$$U_E = \frac{E\,R}{2}\int_0^{2\pi}\int \epsilon^2 dA\, d\alpha \tag{25}$$

where R is the radius of the ring and ϵ is the normal strain of the ring. The normal strain of the ring can be calculated as.

$$\epsilon = \frac{1}{R}\left[-u_1 + \frac{\partial u_2}{\partial \alpha} - \frac{x}{R}\frac{\partial}{\partial \alpha}\left(u_2 + \frac{\partial u_1}{\partial \alpha}\right)\right] \tag{26}$$

The term "x" refers to the distance of a point of the ring from the central axis. As mentioned, the inextensionality of the ring, which makes $\epsilon = 0$ at $x = 0$. Therefore, equation 27 becomes simpler and shows the extensional strain of the ring.

$$u_1 = \frac{\partial u_2}{\partial \alpha} \tag{27}$$

We have the elastic strain energy equation by putting Equations 26 and 27 into equation 25.

$$U_E = \frac{E\,I}{2R^3}\int_0^{2\pi}\left(u_1 + \frac{\partial^2 u_2}{\partial \alpha^2}\right)^2 d\alpha \tag{28}$$

$$U_E = \frac{E\,I\,\pi}{2R^3}\left(9{G_1}^2 + 9{G_2}^2\right) \tag{29}$$

The elastic strain energy equation shows the elliptical modes of the ring and shows that the generalized ring coordinates are not connected in the strain energy equation.

Strain Energy of Semicircular beams

The flexible beams are the integral parts of any MEMS vibrating gyroscope system. The semicircular beams are the supporting structure system to the vibrating ring in the vibrating ring gyroscope system. In Figure 4, the eight semicircular beams are connected to support the ring structure. As we can see, the semicircular beams are relatively small to the ring structure. Therefore, it is considered to neglect the tiny mass of the semicircular beams. In this scenario, the kinetic energy of the semicircular beam could be considered zero.

Preprints.org (www.preprints.org) | NOT PEER-REVIEWED | Posted: 17 July 2024 doi:10.20944/preprints202407.1366.v1

When the force is applied to the vibrating structure, the semicircular beams undergo radial and tangential directions. The semicircular beam radial and tangential stiffnesses considered separately, as shown in Figure 7 [31].

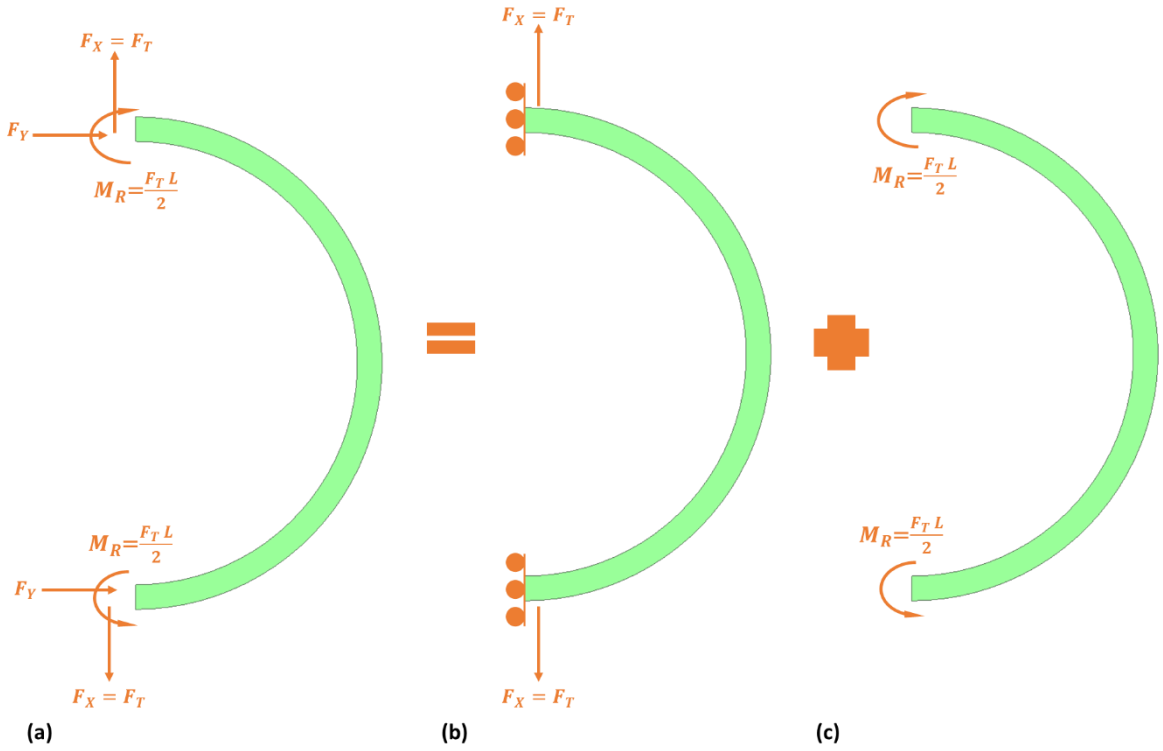

Figure 7. The semicircular support stiffness depiction model (a) complete (b)tangential (c) radial [31].

The strain energy equation determines the stiffness constant for a semicircular beam when subjected to an applied force or an external rotation. This results in tangential and radial displacements, respectively. Therefore, it will be further determined tangential and radial stiffness constant.

The tangential strain energy equation for tangential displacement is represented as equation 30. Where E is Young's modulus, I is the moment of inertia, M is the bending moment experienced, and dx is the differential width of the semicircular beam.

$$U_T = \int \frac{M^2}{2\,E\,I} dx \tag{30}$$

The above equation is further solved [31] and presented as equation 31.

$$U_T = \int_0^{\frac{\pi}{2}} \frac{1}{EI} \left[M_I - \frac{F_T\,R}{2} (1 - \cos\alpha) \right]^2 R\,d\alpha \tag{31}$$

Where F_T is the net applied force, R is the radius of the semicircular support beam, and M_I is the imaginary moment experienced by the semicircular support beam when subjected to the external applied force. Further solving the tangential strain energy equation determines the tangential stiffness constant.

$$\frac{1}{k_T} = \frac{2R^3}{E\,I} \int_0^{\frac{\pi}{2}} \left(\frac{\cos\alpha}{2} - \frac{1}{\pi} \right)^2 d\alpha \tag{32}$$

The radial strain energy equation for radial displacement is represented as equation 33.

Preprints.org (www.preprints.org) | NOT PEER-REVIEWED | Posted: 17 July 2024 doi:10.20944/preprints202407.1366.v1

$$U_T = \int_0^{\frac{\pi}{2}} \frac{{M_R}^2 R}{E\,I} dx \tag{33}$$

The above equation further solved and determined the radial stiffness constant, which is shown as equation 34, where l is the length of the beam.

$$\frac{1}{k_R} = \frac{\pi R l^2}{4EI} \tag{34}$$

The complete stiffness constant equation for the semicircular support beam can be written as.

$$\frac{1}{k_T} + \frac{1}{k_R} = \frac{2R^3}{E\,I} \int_0^{\frac{\pi}{2}} \left(\frac{\cos\alpha}{2} - \frac{1}{\pi}\right)^2 d\alpha + \frac{\pi R l^2}{4EI} \tag{35}$$

There are eight semicircular support beams are attached to the vibrating ring. Therefore, the total strain energy U_{SC} for semicircular beams could be written as equation 36. Where *i*th represents the semicircular support beam position attached to the ring.

$$U_{SC} = \sum_{i=1}^{8} \frac{{u_1}^2}{2} k_R + \sum_{i=1}^{8} \frac{{u_2}^2}{2} k_T \tag{36}$$

By substituting equations 18 and 20 into equation 36, we can further determine the total strain energy U_{SC} for eight semicircular beams attached to the vibrating ring.

$$U_{SC} = \frac{k_R}{2}\left(4{G_1}^2 + 4{G_2}^2\right) + \frac{k_T}{2}\left({G_1}^2 + {G_2}^2\right) \tag{37}$$

Damping Energy

The damping energy for MEMS inertial sensors in the vacuum is generally referred the thermoelastic damping [3,32]. The energy dissipation factor is considered as Rayleigh damping function. The Rayleigh damping function for the MEMS vibrating ring gyroscope system [33] can be expressed as equation 38.

$$R_E = \frac{1}{2}\left[c\left(\left(\frac{dG_1}{dt}\right)^2 + \left(\frac{dG_2}{dt}\right)^2\right)\right] \tag{38}$$

The given expressions $G_1$and G_2 are elliptical mode shapes which are generally represented by 2θ.

To derive the equations of motion for the vibrating internal ring gyroscope, the Lagrange's equation is given as.

$$\frac{d}{dt}\left(\frac{\partial K_E}{\partial \dot{e}_i}\right) - \frac{\partial K_E}{\partial e_i} - \frac{\partial R_E}{\partial \dot{e}_i} - \frac{\partial (U_E + U_{SC})}{\partial e_i} = \frac{\partial E_i}{\partial e_i} \tag{20}$$

The vibrating internal ring gyroscope resonator mechanical model is shown in Figure 4. The derived energy equations will be substituted into equation 20 to find the motion equation of a vibrating ring gyroscope.

$$\frac{5}{8} m\ddot{G_1} + c\dot{G_1} + (4k_R + k_T + \frac{9E\,I\,\pi}{2R^3}) G_{1=}\,\dot{E} \tag{39}$$

$$\frac{5}{8} m\ddot{G_2} + c\dot{G_2} + (4k_R + k_T + \frac{9E\,I\,\pi}{2R^3}) G_{2=}\,\dot{E} \tag{40}$$

To the simplification of the equations of motion for vibrating ring gyroscope, we consider $\frac{5}{8}m = m_G$, $c = c_G$, and $k_G = 4k_R + k_T + \frac{9E\,I\,\pi}{2R^3}$.

Preprints.org (www.preprints.org) | NOT PEER-REVIEWED | Posted: 17 July 2024 doi:10.20944/preprints202407.1366.v1

$$m_G\ddot{G}_1 + c_G\dot{G}_1 + k_G G_{1=} F_1 \quad (41)$$

$$m_G\ddot{G}_2 + c_G\dot{G}_2 + k_G G_{2=} F_2 \quad (42)$$

The natural frequency of the gyroscope is $\omega_G = \sqrt{\frac{k_G}{m_G}}$ and the Quality factor of the gyroscope is $Q_G = \frac{m_G\,\omega_G}{c_G}$. Therefore, the simplified forms of equations of motion for the vibrating ring gyroscope are presented as equations 43 and 44, respectively.

$$\ddot{G}_1 + \frac{\omega_G}{Q_G}\dot{G}_1 + {\omega_G}^2 G_{1=} \frac{F_1}{m_G} \quad (43)$$

$$\ddot{G}_2 + \frac{\omega_G}{Q_G}\dot{G}_2 + {\omega_G}^2 G_{2=} \frac{F_2}{m_G} \quad (44)$$

2.3. Implication of Resonance Analysis on MEMS Vibrating Ring Gyroscope Design

In this section, we will investigate the resonance of elliptical modes of vibrations for MEMS vibrating ring gyroscope. The spring-mass system for MEMs vibrating internal ring gyroscope is shown in Figure 8. The gyroscope system is comprised of the internal vibrating ring mass, spring damper, and externally supported anchors. There are eight support beams attached with the internal vibrating ring mass and the whole vibrating structure system is connected to the externally placed supported anchors.

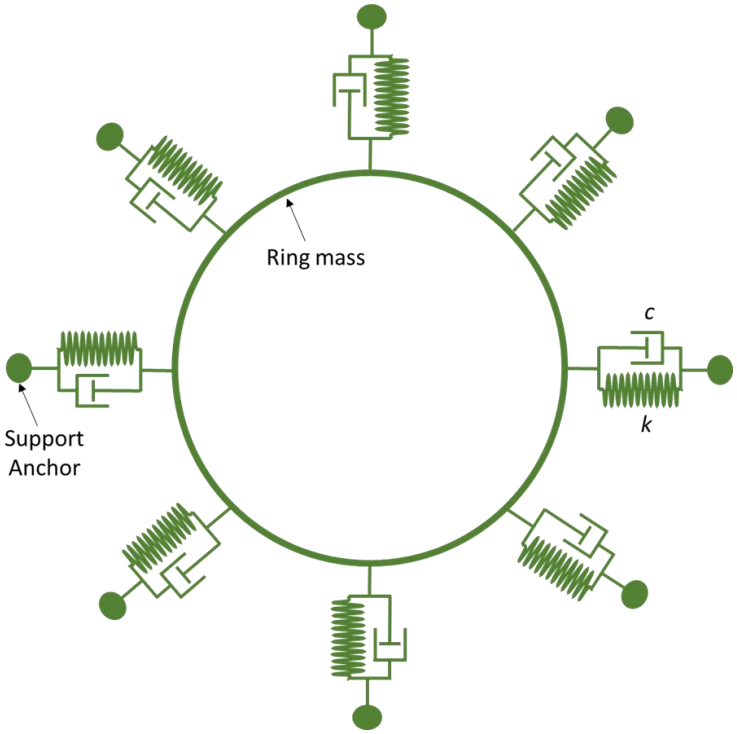

Figure 8. A spring mass damping system for MEMS vibrating internal ring gyroscope.

In the driving operation, the MEMS vibrating ring gyroscope comprised of a single degree of freedom resonator. To understand the driving mechanism of MEMS vibrating ring gyroscope dynamics, it is recommended to consider the 1/8th portion of the ring gyroscope as shown in Figure 9 (b). The 1/8th portion comprised a single resonator of one degree of freedom with one support beam and damping connected to the external anchor. The same concept applies to sensing mechanism too, as the vibrating ring gyroscope comprised of the symmetric design.

Preprints.org (www.preprints.org) | NOT PEER-REVIEWED | Posted: 17 July 2024 doi:10.20944/preprints202407.1366.v1

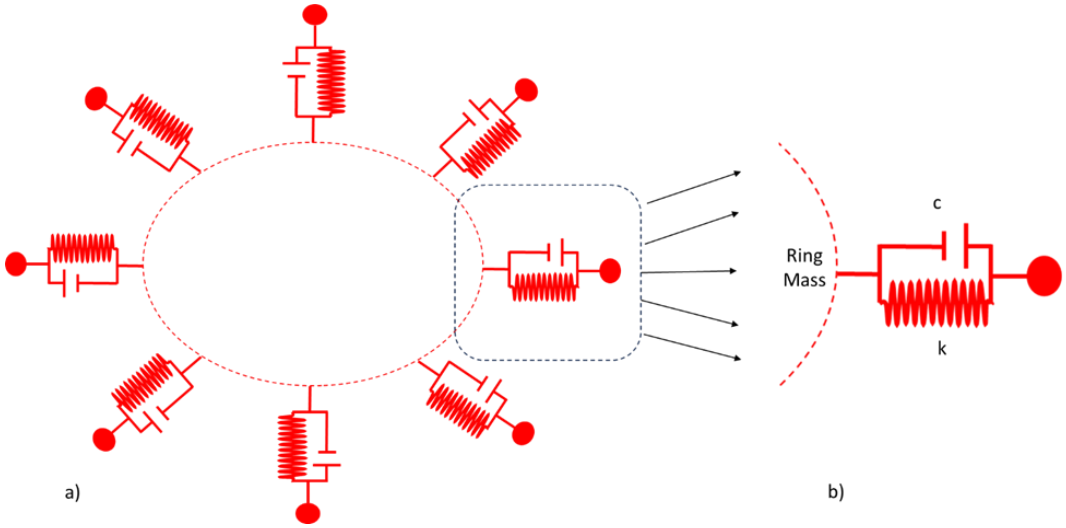

Figure 9. Driving mode of a spring mass system for vibrating ring gyroscope. (a) Complete architecture (b) Single ring resonator.

Let us consider Figure 9 (b); it has a single resonator with one degree of freedom. As previously derived, the equation (26) is implemented on the 1/8th portion of the vibrating ring gyroscope.

$$m_G\ddot{G} + c_G\dot{G} + k_G G = F \tag{45}$$

In further analysis, the natural frequency "ω_N" is a parameter that analyses the oscillation behavior of the vibrating structure without damping. The damping factor "ζ" measures the damping present in the vibrating system relative to the critical damping. The equation of the motion for the 1/8th portion becomes.

$$\ddot{G} + 2\,\zeta\omega_N\dot{G} + {\omega_N}^2 G = \frac{F}{m_G} \tag{46}$$

The Laplace transform function for the single degree of freedom considered to further simplify the equation 46.

$$\frac{G\,(s)}{F\,(s)} = \frac{1}{ms^2 + 2\,\zeta\omega_N s + {\omega_N}^2} \tag{47}$$

When a vibrating ring resonator is subjected to the harmonic force $F = F_0 \sin(\omega t)$ at the given frequency "ω". The system responds with a steady-state harmonic excitation that can be expressed as equation 48.

$$G = G_0 \sin(\omega t + \vartheta) \tag{48}$$

Here "G_0" is the response amplitude and can determined as

$$G_0 = \frac{F_0}{\sqrt{k\left[\left(1 - \left(\frac{\omega}{\omega_N}\right)^2\right)^2 + (2\zeta\frac{\omega}{\omega_N})^2\right]}} \tag{49}$$

$$\vartheta = -\tan^{-1}\left[\frac{2\zeta\omega}{\omega_N} \times \frac{1}{1 - \left(\frac{\omega}{\omega_N}\right)^2}\right] \tag{50}$$

Here F_0 is the amplitude of the applied force, ω is the frequency of the applied force, ω_N is the natural frequency of the vibrating ring, and ϑ is the phase angle between the applied force and the response.

Now, the vibrating ring gyroscope considered as two degrees of freedom resonator, comprising driving and sensing axes. As discussed earlier, the equations of motion for the two degrees of

Preprints.org (www.preprints.org) | NOT PEER-REVIEWED | Posted: 17 July 2024 doi:10.20944/preprints202407.1366.v1

freedom resonator for vibrating ring gyroscope are presented as equations 51 and 52, respectively. The vibrating ring gyroscope oscillates in one direction when there is no rotation applied on to the device.

$$\ddot{G_1} + 2\,\zeta_1\omega_1\dot{G_1} + \omega_1{}^2 G_1 = F_1 \sin(\omega t) \quad (51)$$

$$\ddot{G_2} + 2\,\zeta_2\omega_2\dot{G_2} + \omega_2{}^2 G_2 = 0 \quad (52)$$

In the given situation when no external force is applied to the ring gyroscope's secondary motion. The primary response G_1 and secondary response G_2 of the gyroscope after the closed form solution can be written as equations 53 and 54, respectively.

$$G_1(t) = A_1 e^{-\zeta_1 t}\sin\left(t\omega_1\sqrt{1-\zeta_1{}^2}+\vartheta_1\right) + \frac{F_0}{\sqrt{(\omega_1{}^2-\omega^2)^2+4\zeta_1{}^2\omega_1{}^2\omega^2}}[\sin(\omega t + \tau)] \quad (53)$$

$$G_2(t) = 0 \quad (54)$$

The phase shift "τ" due to the primary oscillation motion can be determined as.

$$\tau = \tan^{-1}\left(\frac{2\zeta_1\omega_1\omega}{\omega_1{}^2-\omega^2}\right) \quad (55)$$

After natural oscillations considered as damped, the equation of solutions 53 and 55 reveals that the frame of the sensitive element, in conjunction with the proof mass, performs forced oscillations along the driving axis with an amplitude corresponding to the excitation force. During this time, the proof mass will not shift away from the driving axis, and therefore, the sensing output will be at zero.

Previously, we considered that there is no rotation when the vibrating ring gyroscope oscillates only in the driving axis. This represents that the oscillation will remain absent in the sensing axis. Now, analyse the behaviour of the vibrating ring gyroscope when it rotates with a constant angular rate. The rotation will bring cross-couplings c_1 and c_2 in both the axes. Therefore, we have effective accelerations a_1 and a_2 due to the external forces applied to the system.

$$\ddot{G_1} + 2\,\zeta_1\omega_1\dot{G_1} + (\omega_1{}^2-\Omega^2)G_1 = a_1 - 2c_1\Omega\dot{G_2} \quad (56)$$

$$\ddot{G_2} + 2\,\zeta_2\omega_2\dot{G_2} + (\omega_2{}^2-\Omega^2)G_2 = a_2 + 2c_2\Omega\dot{G_1} \quad (57)$$

If there are no forces affecting the oscillations in the sensing axis then the $a_2 = 0$ and it will assume there is no coupling between both driving and sensing axes. Hence, sensing oscillation will only work on the angular rate.

The solutions of equations 56 and 57 are of interest due to their role in measuring angular rate, while the natural solution pertains to transient phenomena. If the excitation of the driving oscillation follows a harmonic pattern then the acceleration resulting from the excitation forces can be expressed as equation 58.

$$a_1 = |a_{10}|\cos(\omega t + \vartheta) \quad (58)$$

Here a_1 is the effective acceleration, a_{10} is the amplitude of the effective acceleration, ω is the excitation frequency, and ϑ is the phase constant. The solutions for the driving and sensing oscillations with respect to the decoupling the frame are expressed as equations 59 and 60, respectively.

 doi:10.20944/preprints202407.1366.v1

$$G_1(t) = |A_1|\cos(\omega t + \vartheta_1) \quad (59)$$

$$G_2(t) = |A_2|\cos(\omega t + \vartheta_2) \quad (60)$$

The complex amplitudes related to gyroscope system are defining the forced oscillation at the given frequency A_1 and A_2.

$$A_1 = A_{10}e^{i\vartheta_{10}} \quad (61)$$

$$A_2 = A_{20}e^{i\vartheta_{20}} \quad (62)$$

Now, we have constant amplitudes A_{10}, A_{20} and phases ϑ_{10} , ϑ_{20} for diving and sensing oscillations. The above solutions will substitute in equations 56 and 57.

$$(\omega_1{}^2 - \Omega^2 - \omega^2 + 2\zeta_1 i\omega_1\omega)A_1 + a_1 i\omega\Omega A_2 = a_{10} \quad (63)$$

$$(\omega_2{}^2 - \Omega^2 - \omega^2 + 2\zeta_2 i\omega_2\omega)A_2 - a_2 i\omega\Omega A_1 = 0 \quad (64)$$

To determine the solutions of the complex amplitudes are given below.

$$A_1 = \frac{a_{10}(\omega_2{}^2 - \Omega^2 - \omega^2 + 2\zeta_2 i\omega_2\omega)}{\Delta} \quad (65)$$

$$A_2 = \frac{2c_1 a_{10} i\omega\Omega}{\Delta} \quad (66)$$

$$\Delta = (\omega_1{}^2 - \Omega^2 - \omega^2)(\omega_2{}^2 - \Omega^2 - \omega^2) - (4c_1c_2\omega^2\Omega^2 + 4\zeta_1\zeta_2\omega_1\omega_2\omega^2) + 2i\omega\left[\zeta_1\omega_1\left((\omega_2{}^2 - \Omega^2 - \omega^2\right) + \zeta_2\omega_2((\omega_2{}^2 - \Omega^2 - \omega^2)\right] \quad (67)$$

The phases ϑ_1 and ϑ_2 of the driving and sensing oscillations that correspond to the angles of A_1 and A_2, can be determined by the given equations.

$$\tan(\vartheta_1) = \frac{2\omega\left[\left[\zeta_1\omega_1\left((\omega_2{}^2 - \Omega^2 - \omega^2\right) + \zeta_2\omega_2\left((\omega_1{}^2 - \Omega^2 - \omega^2\right)\right]\left((\omega_2{}^2 - \Omega^2\right.\right.}{(\omega_2{}^2 - \Omega^2 - \omega^2)\left[(\omega_1{}^2 - \Omega^2 - \omega^2)\,(\omega_2{}^2 - \Omega^2 - \omega^2) - \omega^2\Omega^2(c_1c_2 + 4\zeta_1\zeta\right.} \quad (68)$$

$$\tan(\vartheta_2) = \frac{\left[(\omega_1{}^2 - \Omega^2 - \omega^2)\,(\omega_2{}^2 - \Omega^2 - \omega^2) - \omega^2\Omega^2(c_1c_2 + 4\zeta_1\zeta_2\omega_1\omega_2)\right]}{2\omega\left[\zeta_1\omega_1\left((\omega_2{}^2 - \Omega^2 - \omega^2\right) + \zeta_2\omega_2\left((\omega_1{}^2 - \Omega^2 - \omega^2\right)\right]} \quad (69)$$

2.4. Mode Matching in Vibrating Ring Gyroscopes

The vibrating ring gyroscope operates on two primary modes of oscillations, driving oscillations, where the ring continuously vibrates in two orthogonal axes like an elliptical ring. The second vibration mode is sensing oscillations when the device experiences rotation, where the vibrating ring

 doi:10.20944/preprints202407.1366.v1

gyroscope oscillates at 45 degrees between two orthogonal axes and maintains the same elliptical vibration mode [34–38].

In an ideal situation, the driving and sensing resonance frequencies should be matched. This mode matching amplifies the sensing mode response to the angular rate input, making the gyroscope performance more accurate and precise. We consider a case where the vibrating ring gyroscope sensing frequency ω_S is of 10 kHz and has a quality factor Q_f is 1000. At perfect mode matching, the amplification factor of the response is 1000, which is the same as the quality factor. The presented scenario is shown in Figure 10. A vibrating ring gyroscope operates at or close to its resonant frequency and is more susceptible to any fluctuations in the system that shift the resonance frequency. As shown in Figure 10, a 5Hz deviation can cause a significant 29 % loss in the amplification factor. A 10 Hz shift increases to a 55 % loss in the amplification factor.

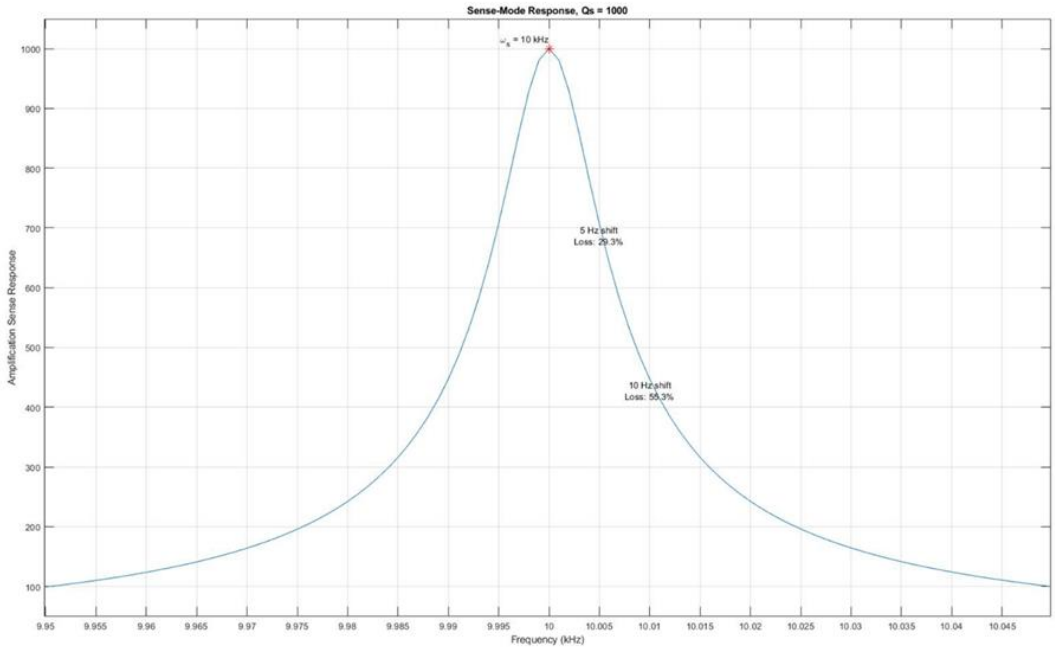

Figure 10. The effect of a resonance frequency shift on the sense mode amplification.

In another scenario, if the quality factor increased to 10000, which gives us a higher amplification factor, it means better results. This also narrows down the operational bandwidth. In this case, if the frequency just shifts 5Hz, it will decrease the gain to 90%, as shown in Figure 11.

 doi:10.20944/preprints202407.1366.v1

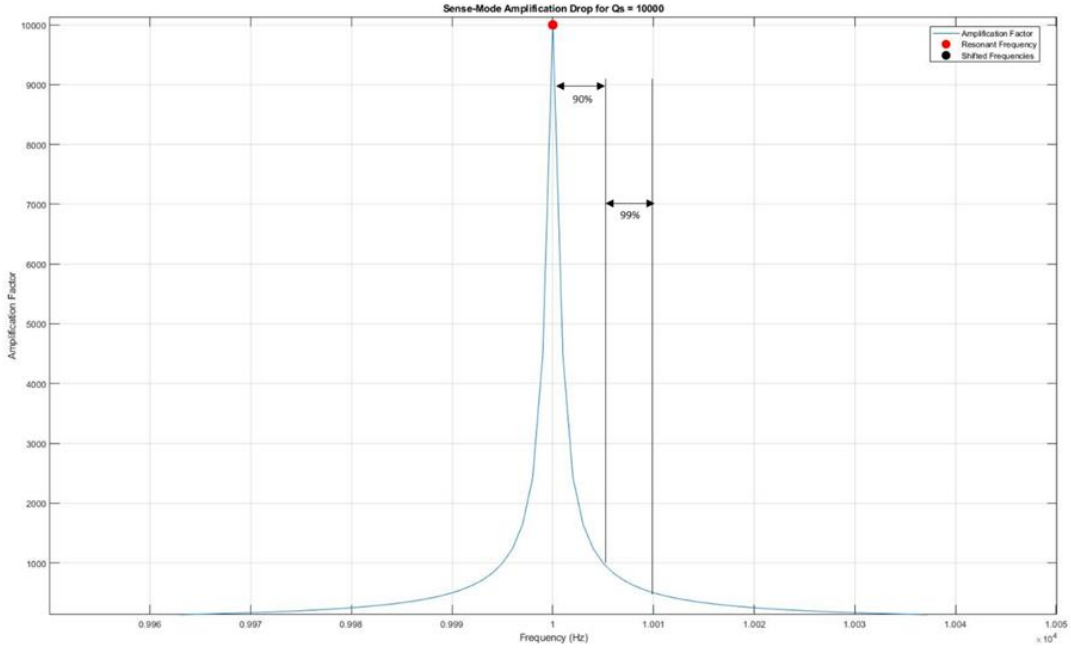

Figure 11. A high-quality factor gyroscope is more susceptible to high loss of gain.

As discussed earlier, operating mode-matched resonance frequencies is quite challenging due to many factors, like unwanted vibrations, microfabrication tolerances, and environmental factors. Therefore, gyroscope operates in the sensing frequency with low peaks is better as it will not impact the sensing amplification factor much. By doing this, the sensing resonance frequency is deliberately offset with a small percentage of the driving resonance frequency. This intentional gap between the driving and sensing resonance frequencies is typically known as a frequency separation system.

Most MEMS vibrating gyroscopes work on the principle of translational motion of single-proof mass system. Translational motion provides better gyroscopic performance and simple microfabrication processes because of single-proof mass system. Some of the gyroscopes utilize the rotational motion of the spring-mass system but add some complex operational processes. On the other hand, dual mass-spring system gyroscopes require more complex microfabrication processes, which sometimes contribute to unwanted errors in the gyroscope operations. The intentional gap between two operating resonance frequencies is represented as equation 70.

$$\Delta f = f_S - f_D \tag{70}$$

3. Conclusion

We presented a thorough investigation of the inplane vibrational dynamics of the MEMS internal vibrating ring gyroscope with semicircular beams. The analysis presented a detailed analytical model of the vibrating ring gyroscope. This includes elliptical vibrational modes assuming inextensional displacements, resulting in detailed equations that could effectively demonstrate a vibrating ring resonator's radial and tangential displacement. The symmetric design structure of the vibrating ring gyroscope provides identical pairs of elliptical vibrational modes. The importance of mode matching on the performance of the gyroscope and disadvantage when sensing frequency has the same peak value as the driving frequency. The derived motion equations are important in order to optimize the design of the vibrating ring gyroscope for increased performance and higher sensitivity.

Author Contributions: The conceptual framework of the MEMS vibrating ring gyroscope was given by K. McKee and I. Howard. The detailed design process, analytical findings, and preparation of the figures were carried out by W. A. Gill. Additionally, W. A. Gill took the lead in writing and reviewing the manuscript,

 doi:10.20944/preprints202407.1366.v1

ensuring the final draft was refined and ready for publication. Supervisory guidance was provided by I. Howard, I. Mazhar, and K. McKee.

Funding: The research support is funded by the Australian government's research training program (RTP) through Curtin University.

Data Availability Statement: Not Applicable.

Conflicts of Interest: The authors declare no conflict of interest.

References

1. Jia J, Ding X, Qin Z, Ruan Z, Li W, Liu X, et al. Overview and analysis of MEMS Coriolis vibratory ring gyroscope. Measurement. 2021;182:109704.
2. Wu X, Xi X, Wu Y, Xiao D. Cylindrical Vibratory Gyroscope: Springer; 2021.
3. Acar C, Shkel A. MEMS vibratory gyroscopes: structural approaches to improve robustness: Springer Science & Business Media; 2008.
4. Apostolyuk V. Theory and design of micromechanical vibratory gyroscopes. MEMS/NEMS: Handbook Techniques and Applications: Springer; 2006. p. 173-95.
5. Li Z, Gao S, Jin L, Liu H, Niu S. Micromachined vibrating ring gyroscope architecture with high-linearity, low quadrature error and improved mode ordering. Sensors. 2020;20(15):4327.
6. Kou Z, Cui X, Cao H, Li B, editors. Analysis and Study of a MEMS Vibrating Ring Gyroscope with High Sensitivity. 2020 IEEE 5th Information Technology and Mechatronics Engineering Conference (ITOEC); 2020. Chongqing, China: IEEE.
7. Syed WU, An BH, Gill WA, Saeed N, Al-Shaibah M, Al Dahmani S, et al. Sensor Design Migration: The Case of a VRG. IEEE Sensors J. 2019;19(22):10336-46.
8. Xia D, Yu C, Kong L. The development of micromachined gyroscope structure and circuitry technology. Sensors. 2014;14(1):1394-473.
9. Passaro VMN, Cuccovillo A, Vaiani L, De Carlo M, Campanella CE. Gyroscope Technology and Applications: A Review in the Industrial Perspective. Sensors. 2017;17(10):2284.
10. Lee JS, An BH, Mansouri M, Yassi HA, Taha I, Gill WA, et al. MEMS vibrating wheel on gimbal gyroscope with high scale factor. Microsyst Technol. 2019;25:4645-50.
11. Liang F, Liang D-D, Qian Y-J. Dynamical analysis of an improved MEMS ring gyroscope encircled by piezoelectric film. International Journal of Mechanical Sciences. 2020;187:105915.
12. Gill WA, Howard I, Mazhar I, McKee K. A Review of MEMS Vibrating Gyroscopes and Their Reliability Issues in Harsh Environments. Sensors. 2022;22(19):7405.
13. Zhang H, Chen W, Yin L, Fu Q. An Interface ASIC Design of MEMS Gyroscope with Analog Closed Loop Driving. Sensors. 2023;23(5):2615.
14. Ma Z, Chen X, Jin X, Jin Y, Zheng X, Jin Z. Effects of Structural Dimension Variation on the Vibration of MEMS Ring-Based Gyroscopes. Micromachines. 2021;12(12):1483.
15. Khan I, Ting DS, Ahamed MJ. Design and development of a MEMS vibrating ring resonator with inner rose petal spring supports. Microsyst Technol. 2021;27:985-95.
16. Xu Q, Hou Z, Kuang Y, Miao T, Ou F, Zhuo M, et al. A tuning fork gyroscope with a polygon-shaped vibration beam. Micromachines. 2019;10(12):813.
17. Nguyen MN, Ha NS, Nguyen LQ, Chu HM, Vu HN. Z-axis micromachined tuning fork gyroscope with low air damping. Micromachines. 2017;8(2):42.
18. Liang F, Liang D-D, Qian Y-J. Nonlinear Performance of MEMS Vibratory Ring Gyroscope. Acta Mechanica Solida Sinica. 2021;34(1):65-78.
19. Gill WA, Ali D, An BH, Syed WU, Saeed N, Al-shaibah M, et al. MEMS multi-vibrating ring gyroscope for space applications. Microsyst Technol. 2020;26:2527-33.
20. Cao H, Liu Y, Kou Z, Zhang Y, Shao X, Gao J, et al. Design, fabrication and experiment of double U-beam MEMS vibration ring gyroscope. Micromachines. 2019;10(3):186.
21. Kou Z, Liu J, Cao H, Shi Y, Ren J, Zhang Y. A novel MEMS S-springs vibrating ring gyroscope with atmosphere package. AIP Advances. 2017;7(12).
22. Gill WA, Howard I, Mazhar I, McKee K. Simulation-Based Design and Analysis for MEMS Vibrating Ring Gyroscope. Engineering Proceedings. 2023;56(1):3.
23. Yoon SW, Lee S, Najafi K. Vibration sensitivity analysis of MEMS vibratory ring gyroscopes. Sensors and Actuators A: Physical. 2011;171(2):163-77.
24. Kou Z, Liu J, Cao H, Han Z, Sun Y, Shi Y, et al. Investigation, modeling, and experiment of an MEMS S-springs vibrating ring gyroscope. Journal of Micro/Nanolithography, MEMS, and MOEMS. 2018;17(1):015001-.
25. Ayazi F, Najafi K, editors. Design and fabrication of high-performance polysilicon vibrating ring gyroscope. Proceedings MEMS 98 IEEE Eleventh Annual International Workshop on Micro Electro

 doi:10.20944/preprints202407.1366.v1

Mechanical Systems An Investigation of Micro Structures, Sensors, Actuators, Machines and Systems (Cat No 98CH36176; 1998: IEEE.
26. Ayazi F, Hsiao H, Kocer F, He G, Najafi K, editors. A High Aspect-Ratio Polysilicon Vibrating Ring Gyroscope. Solid-State Sensor and Actuator Workshop; 2000. Hilton Head Island, South Carolina: IEEE.
27. Shkel AM, Horowitz R, Seshia AA, Park S, Howe RT, editors. Dynamics and control of micromachined gyroscopes. Proceedings of the 1999 American Control Conference (Cat No 99CH36251); 1999: IEEE.
28. He G, Najafi K, editors. A single-crystal silicon vibrating ring gyroscope. Technical Digest MEMS 2002 IEEE International Conference Fifteenth IEEE International Conference on Micro Electro Mechanical Systems (Cat No 02CH37266); 2002: IEEE.
29. Gallacher BJ, Hedley J, Burdess JS, Harris AJ, Rickard A, King DO. Electrostatic correction of structural imperfections present in a microring gyroscope. J Microelectromech Syst. 2005;14(2):221-34.
30. Liu K, Zhang W, Chen W, Li K, Dai F, Cui F, et al. The development of micro-gyroscope technology. Journal of Micromechanics and Microengineering. 2009;19(11):113001.
31. Gill WA, Howard I, Mazhar I, McKee K. Design and Considerations: Microelectromechanical System (MEMS) Vibrating Ring Resonator Gyroscopes. Designs. 2023;7(5):106.
32. Duwel A, Gorman J, Weinstein M, Borenstein J, Ward P. Experimental study of thermoelastic damping in MEMS gyros. Sensors and Actuators A: Physical. 2003;103(1-2):70-5.
33. Wong S, Fox C, McWilliam S. Thermoelastic damping of the in-plane vibration of thin silicon rings. Journal of Sound and Vibration. 2006;293(1-2):266-85.
34. Tsai D-H, Fang W. Design and simulation of a dual-axis sensing decoupled vibratory wheel gyroscope. Sensors and Actuators A: Physical. 2006;126(1):33-40.
35. Hyun An B, Gill WA, Lee JS, Han S, Chang HK, Chatterjee AN, et al. Micro-Electromechanical Vibrating Ring Gyroscope with Structural Mode-Matching in (100) Silicon. sens lett. 2018;16(7):548-51.
36. Zou X, Zhao C, Seshia AA, editors. Edge-anchored mode-matched micromachined gyroscopic disk resonator. 2017 19th International Conference on Solid-State Sensors, Actuators and Microsystems (TRANSDUCERS); 2017: IEEE.
37. Ahn CH, Ng EJ, Hong VA, Yang Y, Lee BJ, Flader I, et al. Mode-matching of wineglass mode disk resonator gyroscope in (100) single crystal silicon. 2014;24(2):343-50.
38. Fan B, Guo S, Cheng M, Yu L, Zhou M, Hu W, et al. Frequency symmetry comparison of cobweb-like disk resonator gyroscope with ring-like disk resonator gyroscope. IEEE Electron Device Letters. 2019;40(9):1515-8.